Role of Single Defects in Electronic Transport through Carbon Nanotube Field-Effect Transistors

Marcus Freitag and A. T. Johnson*

Department of Physics and Astronomy and Laboratory for Research on the Structure of Matter, University of Pennsylvania, 209 South 33rd Street, Philadelphia, Pennsylvania 19104

Sergei V. Kalinin and Dawn A. Bonnell

Department of Materials Science and Engineering, University of Pennsylvania, 3231 Walnut Street, Philadelphia, Pennsylvania 19104

(Received 16 May 2002; published 30 October 2002)

The influence of defects on electron transport in single-wall carbon nanotube field-effect transistors (CNFETs) is probed by combined scanning gate microscopy (SGM) and scanning impedance microscopy (SIM). SGM images are used to quantify the depletion surface potential, and from this the Fermi level, at individual defects along the CNFET length. SIM is used to measure the voltage distribution along the CNFET. When the CNFET is in the conducting state, SIM reveals a uniform potential drop along its length, consistent with diffusive transport. In contrast, when the CNFET is "off," potential steps develop at the position of depleted defects. High-resolution imaging of a second set of weak defects is achieved in a new "tip-gated" SIM mode.

DOI: 10.1103/PhysRevLett.89.216801 PACS numbers: 73.63.Fg, 73.61.Wp, 68.37.Ps

Unique structural and electronic properties of single-wall carbon nanotubes (SWNTs) allow them to act as molecular wires [1] and switching elements in nanoscale devices and logic gates [2–7]. Successful implementation of SWNT electronic devices necessitates quantitative characterization of local structure and properties. Scanning tunneling microscopy resolves local atomic and electronic structure [8], but application to nanotube circuits is problematic because tip current feedback cannot be used when the tip is over an insulating substrate. Local characterization of *active devices* can be done with recently developed techniques such as scanning gate microscopy (SGM) [9,10], electrostatic force microscopy [9], and scanning impedance microscopy (SIM) [11].

Schottky barriers form where semiconducting tubes contact metal electrodes [12,13] or metallic tubes [14]. These barriers can be imaged by SGM and controlled electrostatically by a voltage-biased SGM tip [12,15]. SGM can also resolve valance [9,10] and conduction [6] band potential modulations in carbon nanotube field-effect transistors (CNFETs). These might be associated with atomic defects on the SWNT, e.g., bond rotations, add dimers, or vacancies. Alternatively, they might be ascribed to dopants such as adsorbed or encapsulated impurities [16], or trapped charges in the substrate.

Here we present combined SGM and SIM measurements that illuminate the role of defects on electron transport in CNFETs. Through analysis of electrostatic interactions in SGM, we quantify the depletion surface potential for single defects and the size of their associated valence band modulations, key inputs to the design of CNFET devices. SIM is used to measure the potential distribution in the CNFET at different back-gate voltages. We observe a crossover from diffusive conduction along the full length of the nanotube to conduction inhibited at barriers localized at depleted defects. Finally, we present a SIM mode where the tip simultaneously perturbs the local density and probes the electrostatic potential. This "tip-gating" mode of SIM reveals a set of weak defects that are not resolved in conventional SGM.

Carbon nanotubes are grown by catalytic chemical vapor deposition [17] on a SiO_2/Si substrate. SWNTs are identified by an apparent height less than 3 nm in AFM and then contacted by Cr/Au electrodes defined by *e*-beam lithography. Semiconducting nanotube samples display a strong field effect in response to a back-gate voltage applied to the degenerately doped silicon substrate. Figure 1(a) shows the SGM/SIM measurement setup, based on a Digital Instruments Dimension 3000 NS-IIIA AFM using gold-coated tips (CSC12A, Micromasch). Interleave scans are used for SGM and SIM with a lift height of about 10 nm. CNFET bias voltage V_{ac} is 0.1–1 V_{pp} at a drive frequency a few kilohertz away from the cantilever resonance. To reduce screening due to charge injection from the tube into oxide traps [6,7], the back-gate is triggered by the microscope line-synchronization signal.

In SGM, a conductive tip with an applied potential acts as a spatially localized gate scanned under AFM-feedback near the voltage-biased CNFET. The image formed from the transport current as a function of tip position reveals precise locations where the CNFET has a strong response to the tip gate. We use AC-SGM, with an AC modulation applied to the sample and current measured with a lockin amplifier, significantly reducing measurement noise compared to the DC mode used in earlier work.

 © 2002 The American Physical Society

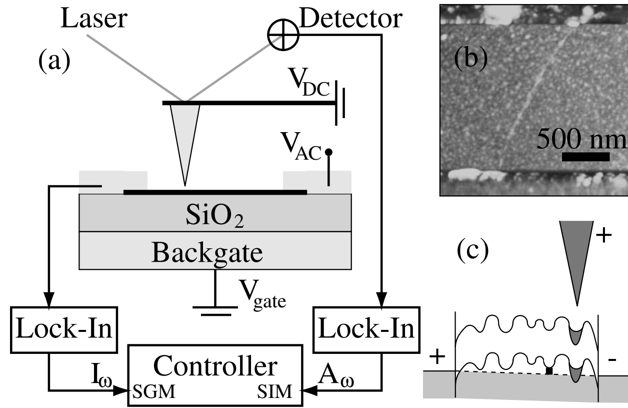

FIG. 1. (a) Setup for scanning gate microscopy (SGM) and scanning impedance microscopy (SIM). In SGM, transport current is measured as a function of tip-gate position. In SIM, the local voltage oscillation is measured. (b) AFM topography image of the CNFET. (c) Schematic of valence band energy modulation due to defects. Vertical black bar is the local Fermi energy. The tip depletes the shaded part of the tube below it.

Our samples are *p*-type CNFETs, so the Schottky barrier at the positively biased electrode is under reverse bias and limits the current. A negatively biased tip positioned near the reverse biased Schottky barrier gives marked current enhancement [12], showing that the barrier can be lowered electrostatically [12,13]. In DC-SGM, only the barrier at the positive electrode is imaged. In AC-SGM, each electrode is at positive bias during half of the AC cycle, and *both* Schottky barriers are imaged (data not shown). At positive bias, the tip probes valence band modulations by depleting carriers (holes) locally. As described in the following paragraphs, images in "depletion mode SGM" are used to quantify the depletion surface potential and Fermi level associated with individual defects.

SGM images at different tip voltages are shown in Figs. 2(a)–2(e). Four strong defects are visible, labeled 1–4. The imaged diameter of each defect increases linearly with tip voltage (Fig. 3). We explain this observation by considering the surface potential distribution below the tip using image charges appropriate for a spherical tip above a dielectric [18]. This approach is applicable for small tip-surface separation, $d \ll R$, where R is the tip radius. We assume that the surface potential is not screened by the nanotube; this is expected if the Debye length in the CNFET is significantly larger than the tube diameter, e.g., when the neighborhood of a defect is nearly depleted. The surface potential below the tip then becomes:

$$V(\rho) = \frac{1}{4\pi\epsilon_0}\frac{2}{\kappa+1}\sum_{i=0}^{\infty}\frac{Q_i}{\sqrt{(R+d-r_i)^2+\rho^2}}, \qquad (1)$$

where ρ is the distance from tip projection on the surface and Q_i a set of image charges located distances r_i from the center of the sphere:

$$Q_{i+1} = \frac{\kappa-1}{\kappa+1}\frac{R}{2(R+d)-r_i}Q_i, \qquad (2)$$

$$r_{i+1} = \frac{R^2}{2(R+d)-r_i}. \qquad (3)$$

R is the tip radius, d the tip-surface separation, $Q_0 = 4\pi\epsilon_0 R V_{\rm tip}$, $r_0 = 0$, $\kappa = 3.9$ the dielectric constant of SiO_2, and $V_{\rm tip}$ the tip bias. For $\rho \gg d, R$ the surface potential becomes $V(\rho) = 2\alpha R V_{\rm tip}/(\kappa+1)\rho$, where α is the ratio of the tip-surface capacitance to that of a sphere of radius R [19]. Current through the CNFET is suppressed at a defect if the local surface potential is $V \geq V^*$, where V^* is the defect depletion surface potential.

The SGM-imaged diameter of the ith defect therefore increases linearly with $V_{\rm tip}$ (Fig. 3): $D_i = (V_{\rm tip}/V_i^*)4\alpha R/(\kappa+1)$. This result lets us determine the relative strength of defects observed in SGM images.

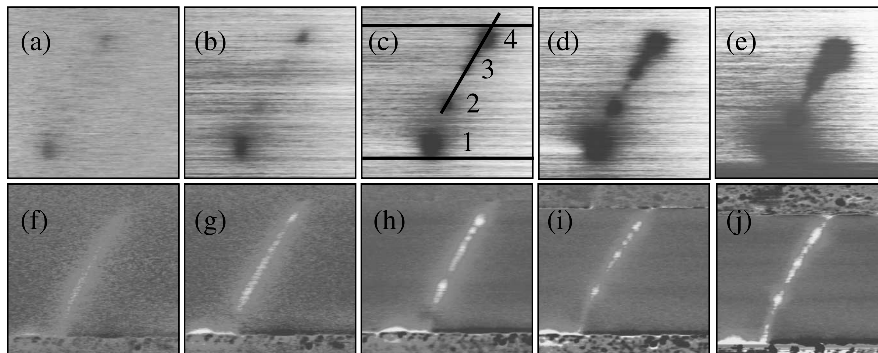

FIG. 2. (a)–(e) SGM images with tip voltage of 1, 2, 4, 6, and 8 V, respectively. Lateral bias is 0.3 V_{pp} for (a)–(c), 0.1 V_{pp} for (d), (e). Back-gate voltage is -1 V. (f)–(j) Simultaneously acquired SIM images. Weak defects are clearly resolved at high tip voltage (see text). Defects 1–4 and the edges of the electrical contacts are shown in (c). The diagonal line in (c) is used for the SIM line scans of Fig. 4.

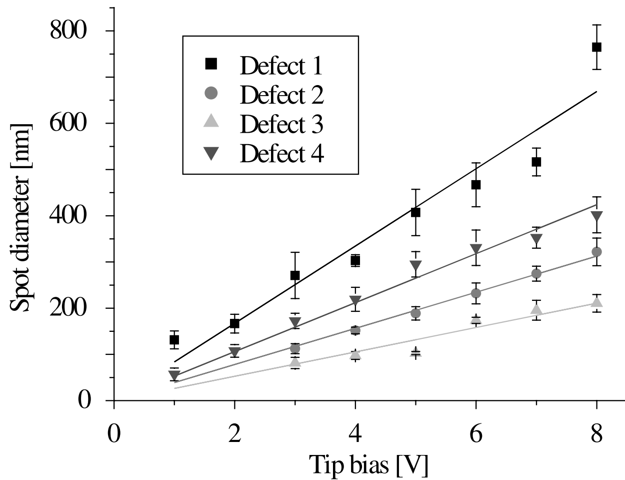

FIG. 3. SGM imaged defect diameter increases linearly with tip voltage. The slope of the line gives the depletion surface potential of each defect.

The largest uncertainty in the absolute depletion surface potential V_i^* of a given defect is the tip radius of curvature R, taken to be 20 nm. The capacitance ratio α can be calculated for known tip geometries and varies weakly $\alpha = 1.0$–1.5 for tip radii from ten to 100 nm, and tip-surface separations of 1–100 nm; we take $\alpha \sim 1.1$ as a representative value. For the strong defects (numbered 1–4) seen in Figs. 2(a)–2(e), we find depletion surface potentials of 220, 460, 680, and 340 meV, respectively, with uncertainties from data fitting of 10–20 meV. The two strongest defects are close to the electrodes, suggesting that the Schottky barriers at the contacts lead to additional band bending that enhances the impact of nearby defects.

The measured depletion surface potential can be converted into an estimate of the local Fermi energy near the defect with $V_{\text{tip}} = 0$. As carriers are added to the depleted region, both the electrostatic potential, Φ, and the Fermi energy, ϵ_F, increase. With N carriers added to a region of length l, these become $e\Phi = Ne^2/Cl$, and $\epsilon_F = N/Dl$, where C is the total capacitance of the region per unit length, and D is the density of states per unit length, assumed constant for clarity. We estimate the capacitance from a coaxial geometry [$C \sim 2\pi\epsilon\epsilon_0/\ln(2h/r) \sim 30$ pF/m $= 0.2$ e/V-nm, where $h = 200$ nm is the oxide thickness and $r = 1$ nm the CNFET radius [3]] and compare it to the "quantum capacitance"[20] $e^2D = 2.4$ e/V-nm, assuming four-fold level degeneracy (spin and subband) and Fermi velocity $\hbar v_F = 0.5$ eV-nm, appropriate for metallic nanotubes. Semiconducting tubes have a larger density of states near the band edge but approach this value away from the van Hove singularity. The ratio $C/e^2D = 1/12$ leads to an estimated Fermi energy of 20, 35, 50, and 25 meV for the strong defects 1–4 in Fig. 2(a)–2(e).

To further characterize defect related transport properties of the nanotube, we perform simultaneous SIM [Ref. [11]; schematic Fig. 1(a)] to determine the local potential along the CNFET length. The tip and backgate are held at constant voltages V_{tip} and V_g. A lateral bias: $V_{\text{lat}} = V_{\text{dc}} + V_{\text{ac}}\cos(\omega t)$ is applied to the sample to give an oscillating surface potential $V_{\text{surf}} = V_s + V_{\text{ac}}(x)\cos[(\omega t) + \varphi(x)]$, where $V_{\text{ac}}(x)$ and $\varphi(x)$ are the amplitude and phase shift of the voltage oscillation, and V_s the dc surface potential. The first harmonic of the electrostatic force on the tip is directly proportional to $V_{\text{ac}}(x)$, and the amplitude and phase shift signal from the cantilever reflect the amplitude and phase of the surface potential oscillation [11].

When biased at a small negative voltage (e.g., $V_{\text{tip}} = -1$ V), the tip slightly enhances the local carrier density but acts as a weakly invasive probe of the potential distribution. In Fig. 4(a) we see that when the CNFET is off (poorly conducting, transport current 40 nA) at $V_g = +0.7$ V, SIM shows clearly resolved potential steps at defects 2 and 4, while a series of weaker scattering centers gives a uniform voltage increase in the neighborhood of defect 3. The nanotube is divided into multiple conducting segments separated by distinct barriers at stronger defects. Figure 4(b) shows that SIM indicates a *uniform potential drop* along the device when the CNFET is on (conducting, transport current 350 nA) with $V_g = 0$ V. All defects are far from depletion, and each acts as a weak scatterering site: transport along the CNFET is diffusive. We have reported evidence for ballistic transport in semiconducting nanotubes at very high electrostatic doping [6,21]. SIM measurements in this regime are in progress and will be reported elsewhere.

Figures 2(d) and 2(e) show that the large SGM signal from defects three and four obscure a set of weak defects that lie between these two. These weaker defects can be

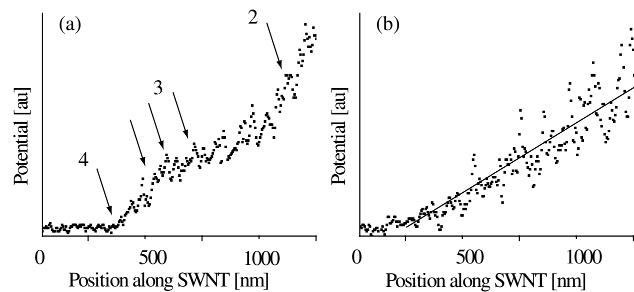

FIG. 4. (a) When the CNFET is in the "off" state, SIM shows voltage steps at the position of strong defects. The bias, backgate, and tip voltages are $V_{\text{ac}} = 0.1\ V_{pp}$, $V_g = 0.7$ V, and $V_{\text{tip}} = -1$ V. The lateral bias is $V_{\text{ac}} = 0.1\ V_{pp}$. At the voltage of $V_{\text{tip}} = -1$ V the tip is a noninvasive probe. (b) SIM images a uniformly increasing potential along the CNFET in the "on" state (backgate = 0 V). The line for both scans is indicated in Fig. 2(c).

studied using a "tip-gated" SIM mode with a large positive voltage applied to the tip gate. At this voltage, the tip gate strongly alters the density and voltage profile beneath it. If the tip voltage is sufficient to deplete a defect, a potential step is created at the defect site, resulting in a large SIM signal when the tip is precisely above the defect, with a sharp reduction in signal as the tip moves away. This "tip-gating" mode enables high-resolution imaging of weak defects, even if they lie near other stronger defects [Figs. 2(i) and 2(j)]. This approach is extremely effective in detecting weak defects and will be used in future experiments to determine their associated Fermi energies.

In conclusion, we have studied defects in semiconducting SWNTs by AC-SGM and SIM. The imaged defect size in SGM increases linearly with tip potential, in agreement with an analysis of the electrostatic interactions. This is used to determine the depletion surface potential and Fermi energy for individual defects, ranging from 220–680 meV and 20–55 meV, respectively, for the strong defects observed in this experiment. SIM shows a series of potential drops located at defect sites when the CNFET is in the off state, and a uniform potential drop along the CNFET, indicative of diffusive conduction, when it is in the on state. Finally, a novel self-gating SIM mode is used to image defects with enhanced resolution even when they are weak and located close to strong defects.

We acknowledge the support from MRSEC Grant No. NSF DMR 00-79909 and valuable discussions with M. Cohen, E. J. Mele, and M. Radosavljević.

---

*Electronic address: cjohnson@physics.upenn.edu

[1] S. J. Tans, M. H. Devoret, H. Dai, A. Thess, R. E. Smalley, L. J. Geerligs, and C. Dekker, Nature (London) **386**, 474 (1997).

[2] S. J. Tans, A. R. M. Verschueren, and C. Dekker, Nature (London) **393**, 49 (1998).

[3] R. Martel, T. Schmidt, H. R. Shea, T. Hertel, and P. Avouris, Appl. Phys. Lett. **73**, 2447 (1998).

[4] V. Derycke, R. Martel, J. Appenzeller, and Ph. Avouris, Nano Lett. **1**, 453 (2001).

[5] A. Bachtold, P. Hadley, T. Nakanishi, and C. Dekker, Science **294**, 1317 (2001).

[6] M. Radosavljevic, M. Freitag, K.V. Thadani, and A.T. Johnson, Nano Lett. **2**, 761 (2002).

[7] M. Fuhrer, B. M. Kim, T. Durkop, and T. Brintlinger, Nano Lett. **2**, 755 (2002).

[8] J.W. G. Wildoer, L.C. Venema, A.G. Rinzler, R.E. Smalley, and C. Dekker, Nature (London) **391**, 59 (1998); T.W. Odom, J.L Huang, P. Kim, and C.M. Lieber, Nature (London) **391**, 62 (1998).

[9] A. Bachtold *et al.*, Phys. Rev. Lett. **84**, 6082 (2000).

[10] S. J. Tans and C. Dekker, Nature (London) **404**, 834 (2000); M. Freitag, M. Radosavljevic, W. Clauss, and A. T. Johnson, Phys. Rev. B **62**, R2307 (2000).

[11] S.V. Kalinin and D. A. Bonnell, Appl. Phys. Lett. **78**, 1306 (2001).

[12] M. Freitag, M. Radosavljević, Y. Zhou, A. T. Johnson, and W. F. Smith, Appl. Phys. Lett. **79**, 3326 (2001).

[13] S. Heinze, J. Tersoff, R. Martel, V. Derycke, J. Appenzeller, and Ph. Avouris, Phys. Rev. Lett. **89**, 106801 (2002).

[14] M. Fuhrer, J. Nygard, L. Shih, M. Forero, Young-Gui Yoon, m. S. C. Mazzoni, H. J. Choi, J. Ihm, S. G. Louie, A. Zettl, and P. L. McEuen, Science **288**, 494 (2000).

[15] M. Freitag and A.T. Johnson, in Materials Research Society Symposium Proceedings of the Fall Meeting 2001 (2001), Vol. 706, p. 371.

[16] D. J. Hornbaker, S.-J. Kahng, S. Misra, B.W. Smith, A. T. Johnson, E. J. Mele, D. E. Luzzi, and A. Yazdani, Science **295**, 828 (2002).

[17] J. Kong, H. T. Soh, A. M. Cassell, C. F. Quate, and H. Dai, Nature (London) **395**, 878 (1998); J. H. Hafner, C. L. Cheung, and C. M. Lieber, Nature (London) **398**, 761 (1999).

[18] J. D. Jackson, *Classical Electrodynamics* (John Wiley, New York, 1998).

[19] S V. Kalinin, M. Freitag, A.T. Johnson, and D. A. Bonnell (unpublished).

[20] S. Luryi, Appl. Phys. Lett. **52**, 501 (1988).

[21] A.T. Johnson, in Proceedings of the 2002 Meeting of the Electrochemical Society, Fullerenes, Vol. 12 (to be published).